Maximum entropy inference of seabed properties using waveguide invariant features from surface ships

D. P. Knobles, T. B. Neilsen, P. S. Wilson, et al.

Citation: The Journal of the Acoustical Society of America **151**, 2885 (2022); doi: 10.1121/10.0010372
View online: https://doi.org/10.1121/10.0010372
View Table of Contents: https://asa.scitation.org/toc/jas/151/5
Published by the Acoustical Society of America

ARTICLES YOU MAY BE INTERESTED IN

Robust shallow water reverberation reduction methods based on low-rank and sparsity decomposition
The Journal of the Acoustical Society of America **151**, 2826 (2022); https://doi.org/10.1121/10.0010353

Adaptive equalization based on dynamic compressive sensing for single-carrier multiple-input multiple-output underwater acoustic communications
The Journal of the Acoustical Society of America **151**, 2877 (2022); https://doi.org/10.1121/10.0010370

Effect of alternate definitions of “high” annoyance on exposure-response functions
The Journal of the Acoustical Society of America **151**, 2856 (2022); https://doi.org/10.1121/10.0010354

Pioneering study of outdoor sound propagation
The Journal of the Acoustical Society of America **151**, R11 (2022); https://doi.org/10.1121/10.0010350

Dual-path transformer-based network with equalization-generation components prediction for flexible vibrational sensor speech enhancement in the time domain
The Journal of the Acoustical Society of America **151**, 2814 (2022); https://doi.org/10.1121/10.0010316

Reviews of Acoustical Patents
The Journal of the Acoustical Society of America **151**, 2809 (2022); https://doi.org/10.1121/10.0010351

ASA POMA Proceedings of Meetings on Acoustics
Why Publish in POMA?
Watch Now

JASA ARTICLE

Maximum entropy inference of seabed properties using waveguide invariant features from surface ships

D. P. Knobles,[1,a] T. B. Neilsen,[2] P. S. Wilson,[3] W. S. Hodgkiss,[4] J. Bonnel,[5] and Y. T. Lin[5]

[1]*Knobles Scientific and Analysis, Austin, Texas 78755, USA*

[2]*Department of Physics, Brigham Young University, Provo, Utah 84604, USA*

[3]*Mechanical Engineering Department and Applied Research Laboratories, University of Texas, Austin, Texas 78713, USA*

[4]*Marine Physical Laboratory, Scripps Institution of Oceanography, University of California, San Diego, La Jolla, California 92093, USA*

[5]*Woods Hole Oceanographic Institute, Falmouth, Massachusetts 02543, USA*

ABSTRACT:

Acoustic data were recorded on two vertical line arrays (VLAs) deployed in the New England Mud Patch during the Seabed Characterization Experiment 2017 in about 75 m of water. The sound recorded during the passage of merchant ships permits identification of singular points for the waveguide invariant β for mode pairs $(1,n):\beta_{1,n}$, for $n = 2, 3, 4, 5$, in the 15–80 Hz band. Using prior geophysical information and an acoustic data sample from the merchant ship *KALAMATA*, a geoacoustic model $\mathfrak{M}$ of the seabed was developed. Then, using data samples from other merchant ships, a *feature-ensemble* maximum entropy method is employed to infer the statistical properties of geoacoustic parameter values for the sound speeds in a surface mud layer and a deep sand layer. Technical challenges include a sparsity of observed singular points, the unique identification of mode pairs for an observed singular point, and the deviation of the waveguide from horizontal stratification. A geoacoustic model $\mathfrak{M}$ is developed that reproduced the observed $\beta \approx -1$ for $f < 20$ Hz and mode cutoff features at about 15 Hz. The statistical low-frequency inference of the singular point structure from multiple ships provides evidence of an angle of intromission at the water sediment interface with an average sound speed ratio of about 0.986 and an average sound speed for the deeper sand layer of about 1775 m/s. © *2022 Acoustical Society of America*. https://doi.org/10.1121/10.0010372

(Received 2 January 2022; revised 12 April 2022; accepted 13 April 2022; published online 28 April 2022)

[Editor: Kay L. Gemba] Pages: 2885–2896

I. INTRODUCTION

A motif in seabed acoustics links characteristics of the seabed to physical quantities, such as orthogonal normal mode depth functions and their horizontal wavenumber eigenvalues,[1–3] which can facilitate an interpretation of the observed acoustic field. Spatial correlation of wind noise[4–7] can also reveal certain characteristics of the seabed. Such physics-based methodologies elucidate the nature of broadband transmission loss in shallow water in terms of modal dispersion properties. A previous analysis[8] inferred that the waveguide invariant for modal pairs 1 and 2 ($\beta_{1,2}$) had a singular point, i.e., $\beta_{1,2}(\mathcal{F}) = \infty$ at $\mathcal{F} \approx 25$ Hz. This deduction was made from acoustic data recorded on a 16-element Marine Physical Laboratory (MPL) vertical line array (VLA) during the Seabed Characterization Experiment (SBCEXP) 2017 in the central region of the New England Mud Patch.[9] A *feature*-based inversion method correlated the observed value of $\mathcal{F}$ to the characteristics of a water-saturated layer that lies beneath the first 20 m of sediment. A more careful perusal of the recorded low-frequency sound from multiple merchant ships revealed additional singular points of $\beta_{m,n}$ forming a pattern and also regions where β changes sign.

This paper endeavors to connect the concept of statistical inference of seabed properties to selected observed features of the waveguide invariant in merchant ship spectrograms. The general idea of a Bayesian method using feature-based matching is not new (see, for example, Ref. 10). The supposition is that if enough features are extracted from measured ship spectrograms, then one can develop a likelihood function with which to generate meaningful probability distributions for selected parameter values of a geoacoustic model of the seabed. The current work performs a constrained statistical feature-based inversion via the singular points of $\beta_{m,n}$. Singular points of objects are often used for classification. For example, all linear differential equations in physics can be classified by their singular points.[11]

An advantage of using the singular points in an inversion scheme for seabed properties is that they do not depend on source-receiver range, ship speed, source depth, and receiver depth. Rather, the locations of the singular points depend only on the properties of the waveguide. Once the singular points are used to estimate the geoacoustic profile, the frequency dependent interference pattern at closest point of approach (CPA) time, which is independent of the ship speed, can be used to estimate the CPA range. Then the ship speed can be estimated by matching several main striation patterns over a larger portion of the frequency-time spectrogram.

[a]Electronic mail: dpknobles.kphysics.org

The remainder of this paper is organized as follows. Section II shows the experimental area and tracks of merchant ships and selected observations of singular points of $\beta_{m,n}$. Section III provides a formulation for the idea of feature-based statistical inference that utilizes singular points of $\beta_{m,n}$. Section IV presents the results of the analysis. A preliminary geoacoustic model is utilized to identify the mode pairs associated with these observed singularities of $\beta_{m,n}(f)$. Multiple observed singular values in $\beta_{m,n}(f)$ and other low-frequency features are identified from the low-frequency sound emitted by four merchant ships. The observed mode cutoff frequency for mode numbers >1 provides a constraint for the geoacoustic model. Then a data ensemble maximum entropy analysis that uses data provides statistics for geoacoustic parameter values of a geoacoustic model. Section V provides a summary.

II. EXPERIMENTAL AREA AND SAMPLING OF MEASUREMENTS

Many surface ships were detected during SBCEXP 2017. Figure 1(a) shows the tracks of two merchant ships, the vehicle carrier *VIKING BRAVERY* [International Maritime Organization (IMO) 9673020/Maritime Mobile Service Identity (MMSI) 565806000] and the *KALAMATA* (IMO 9244946/MMSI 477510600) relative to two MPL VLAs. The two VLAs were separated by about 6.7 km and placed on the central northwest (NW) to southeast (SE) channel of the Mud Patch,[12] where a surficial layer of mud had its largest thickness. An example of the thickness in two-way travel times is shown in Figs. 1(b) and 1(c) for a track that is close to the line connecting the two VLAs. Most of the acoustic and survey measurements for SBCEXP 2017 were concentrated along the NW to SE track.[13,14] The bathymetry along the NW to SE track was approximately constant at 75 m. Merchant shipping lanes defined both the northern and southern boundaries of the SBCEXP 2017 experimental area with the container ship *KALAMATA* in the southern shipping lane. Most of the data of interest are from merchant ships in the southern shipping lane because of its proximity to VLA 2. The ocean waveguide (including the seabed) generally does not possess horizontal stratification from points on the track of ships in the southern shipping lane to VLA 1 and VLA 2. The sound recordings of the *VIKING BRAVERY* were a fortuitous measurement because its track was along the main NW to SE channel of mud.

As an example of ship spectrograms at the low frequencies (<100 Hz), Fig. 2 shows time-frequency spectrograms on VLA 2 from processed data recorded during the passage of the *KALAMATA*. The spectrograms were produced using the CHIRP Z transform[15] on the pressure time series with an integration time T of approximately 84 s. The time window selected for each spectrogram is such that the CPA time is at the center of the observation time interval. Processing the data with a fine frequency resolution $\delta f = 1/T$ permitted the $\beta = \infty$ discovery made in Ref. 8. White dashed lines identify points where the slope of the intensity striation vanishes, which is the condition for a singular point for $\beta_{m,n}$. It follows from the analysis in Ref. 8 that the white dashed lines are apparent singular points of $\beta_{n,m}$. Ordinarily, making a correlation between an observed singular point and a specific mode pair requires the ability to model the spectrogram and the corresponding group velocity or $\beta_{m,n}$.

The sound recordings of the *KALAMATA* are of significant interest to this study because for $f<25$ Hz, striations with $\beta \approx -1$ are evident down to about 14 Hz. The red dashed line in Figs. 2(a) and 2(b) is positioned at about 13.8 Hz, below which there are no observed striations. This area of the spectrum also possesses discrete lines. One can conclude that for $f<14$ Hz, modes with mode numbers >1 are in the evanescent part of the modal spectrum. This very low-frequency (VLF) observation permits the conjecture of an effective geoacoustic model with a fixed very deep structure that reproduces this cutoff feature, independent of modifications to sediment layers at shallower depths.

Figure 3 provides additional examples from different receiver depths of apparent singular points from the *KALAMATA*. Figure 3(a) shows a spectrogram possessing

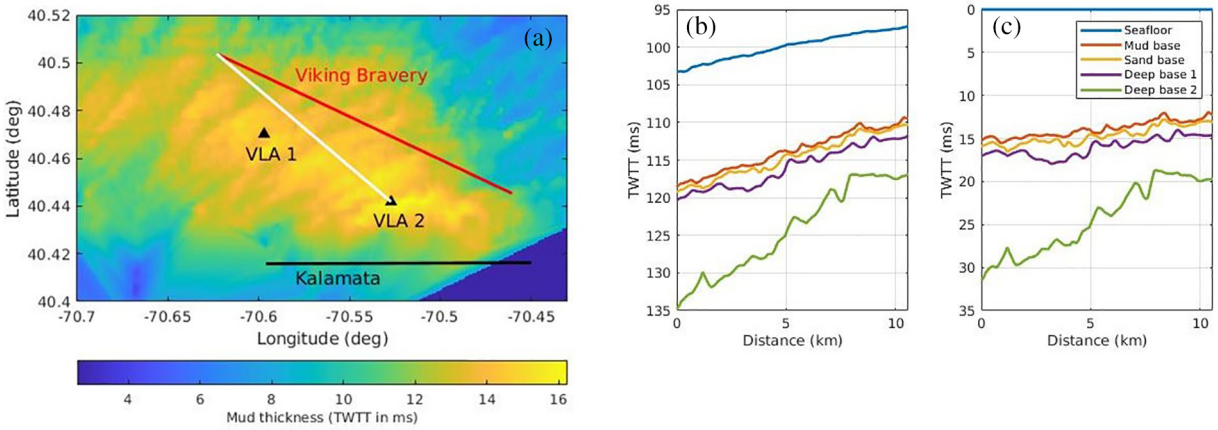

FIG. 1. (Color online) (a) Tracks of merchant ships *VIKING BRAVERY* and *KALAMATA* during SBCEXP 2017 in the New England Mud Patch. (b) Two-way travel times (TWTT) for seafloor and various sediment layers along a white colored track from a subbottom survey (Ref. 13). (c) Two-way travel times relative to the seafloor.

https://doi.org/10.1121/10.0010372

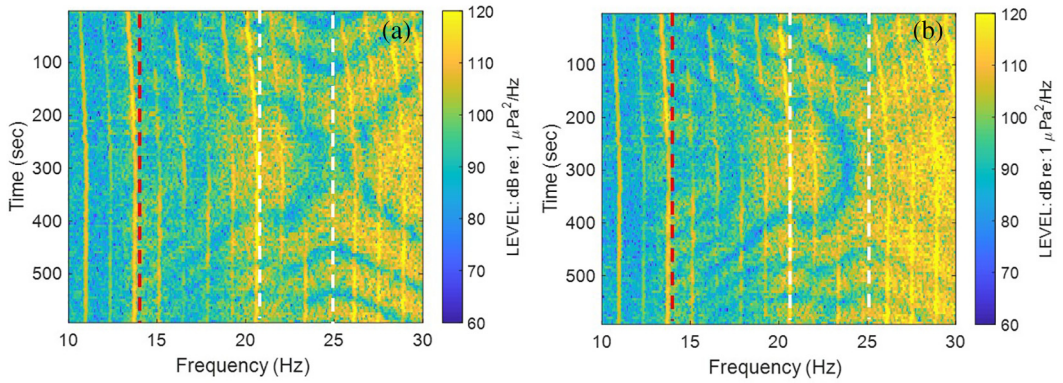

FIG. 2. (Color online) Spectrograms made from sound recordings on VLA 2 during the passage of the container ship *KALAMATA* on day 83, hour 18, minutes 26–35: (a) hydrophone receiver depth 41.20 m and (b) hydrophone receiver depth 29.95 m. White dotted lines indicate an apparent singular point of $\beta_{m,n}$, and the red dotted line indicates a frequency below which modal interference vanishes.

three singularities at about 25, 35, and 41 Hz. In the proximity of the 35 Hz singularity, there exists an apparent distribution of $\beta_{m,n}$ with differing striation slopes creating a complicated pattern. Figure 3(b) shows a singular point at about 53 Hz with the main striation splitting into multiple sub-striations, giving the appearance of a *bird in flight*. Not all the apparent singular points of $\beta_{n,m}$ are observable on a specific hydrophone of the VLA. For example, the apparent singular point at about 41 Hz can be seen at a receiver depth of 44.95 m in Fig. 3(a) but not at a receiver depth of 29.95 m in Fig. 3(b). The higher order singular points $\beta_{1,n}$ for $n > 2$ are easier to observe on receivers located nearest to the null for mode 2.

The sound recordings of the *KALAMATA* are used to (1) develop a means by which to associate mode pairs with observed singularities and (2) set parameters for the very deep portions of the seabed using a fortuitous observation of a mode cutoff feature at about 15 Hz.

The sound recordings on VLA 2 from four ships other than the *KALAMATA* were selected for the maximum entropy analysis, specifically, the tanker *MAERSK MATSUYAMA* (IMO 9367736/MMSI 370514000), the chemical oil tanker *TORM CORRIEDO* (IMO 9411305/MMSI 219028420), the chemical oil tanker *HAFNIA GREEN* (IMO: 9360441/MMSI: 565978000), and the *VIKING BRAVERY*. These ships, like the *KALAMATA*, possess examples of apparent singular points of $\beta_{m,n}$ in the $15 < f < 80$ Hz band. The difficult question that first needs to be addressed in formulating a statistical feature-based inverse problem is how to assign specific mode pairs to the observed apparent singular points.

III. MATHEMATICAL DEVELOPMENT

This section presents the mathematical formulation for (1) simulation of the observed time-frequency spectrogram of surface ship recordings, (2) the waveguide invariant $\beta_{m,n}$ for pairs of modes, and (3) data ensemble feature-based maximum entropy.

A. Simulation of acoustic field

The Green's function $\mathcal{G}$ solution to the Helmholtz equation for a unit point source undergoing uniform motion at a speed of V along a track of length L in a horizontally stratified ocean environment is solved by a normal mode expansion,

$$\mathcal{G}(f, z_s, z, R(t)) = \frac{i}{4\rho(z_s)} \sum_m \phi_m(z_s)\phi_m(z) H_0^1(k_m R(t)), \qquad (1)$$

where k_m and ϕ_m are the horizontal wavenumber eigenvalues and depth dependent wavefunctions, respectively.

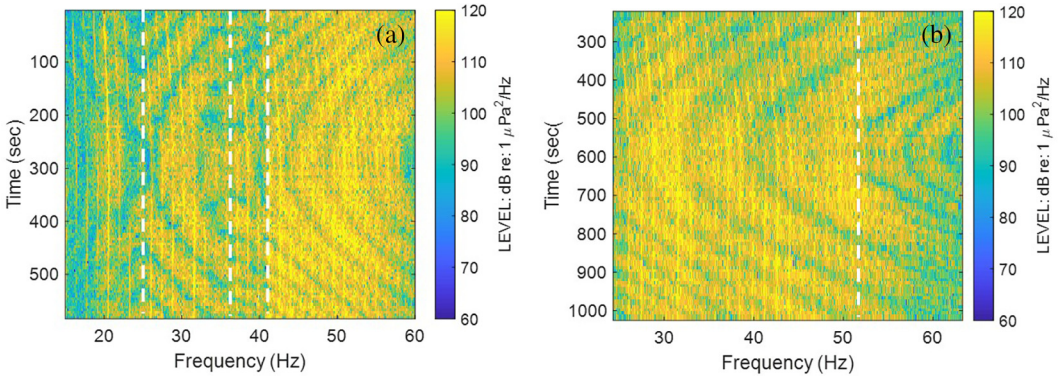

FIG. 3. (Color online) Spectrograms made from sound recordings on VLA 2 during the passage of the container ship *KALAMATA* on day 83, hour 20, minutes 50–72: (a) hydrophone receiver depth 44.95 m and (b) hydrophone receiver depth 29.95 m. White dotted lines indicate an apparent singular point of $\beta_{m,n}$.

Doppler effects have been neglected. The modeled transmission loss (TL_{mod}) is

$$TL_{mod}((f, z_s, z, R(t))) = 20\ \log_{10}\left(\text{abs}(\mathcal{G}(f, z_s, z, R(t))\right). \quad (2)$$

The complex pressure is modeled as

$$\hat{P}(f, z_s, z, R(t')) = \hat{S}(f)\mathcal{G}(f, z_s, z, R(t)), \quad (3)$$

where $\hat{S}(f)$ is the complex source function, generally unknown, of the surface ship. The received level (RL) and the source level (SL) are defined as

$$RL_{mod}(f, z_s, z, R(t')) = 20\log_{10}(\text{abs}(\hat{P}(f, z_s, z, R(t'))) \quad (4)$$

and

$$SL(f) = 20\log_{10}(\text{abs}(\hat{S}(f))) \quad (5)$$

with

$$RL_{mod}(f, z_s, z, R(t')) = SL(f) + TL_{mod}(f, z_s, z, R(t')). \quad (6)$$

In the implicit formulation of SL, an error function $\mathcal{E}$ of a squared error form,

$$\mathcal{E} = \frac{1}{N_f N_T N_z}\sum_i\sum_j\sum_k (RL_{mea}(f_i, z_j, t_k) - (SL(f_i) - TL_{mod}(f_i, z_j, t_k)))^2, \quad (7)$$

is used to determine the source level from the condition

$$\frac{\partial \mathcal{E}}{\partial SL} = 0, \quad (8)$$

which leads to

$$SL(f_i) = \frac{1}{N_T}\frac{1}{N_{zr}}\sum_k\sum_j (RL_{mea}(f_i, z_j, t_k) + TL_{mod}(f_i, z_j, t_k)). \quad (9)$$

Insertion of Eq. (9) into Eq. (6) gives

$$RL_{mod}(f_i, z_j, t_k) = SL(f_i) + TL_{mod}(f_i, z_j, t_k). \quad (10)$$

In a numerical implementation of Eqs. (1)–(10), RL_{mod} is generally computed over a finite frequency bandwidth at discrete frequencies $f_i, i = 1, 2, \ldots, N_f$, where $f_{i+1} - f_i = \Delta f$.

B. Waveguide invariant for pair of modes

The characteristics of β in ocean waveguides have received significant interest in ocean acoustics over the past 2 decades.[16–22] In shallow water, where reflection from the top and seabed boundaries characterize the waveguide, $\beta \approx 1$, especially for isospeed conditions. However, when the seabed is penetrable with multiple layers of varying physical properties, such as that which describes the NE Mud Patch, one can expect $\beta_{n,m}$ to exhibit a complex behavior as a function of frequency and mode number pairs (n,m). The inversion idea adopted in Ref. 8 was a matched-feature approach to find optimal values for a deep sediment layer that would produce the observed singular point of $\beta_{1,2}(\mathcal{F})$. Here, we extend the original idea to the case

$$\vec{\mathfrak{F}}_\ell = ({}^\ell\mathcal{F}_1, {}^\ell\mathcal{F}_2, {}^\ell\mathcal{F}_3, \ldots, {}^\ell\mathcal{F}_K), \quad (11)$$

where K is the number of observed singular points that can be correlated or matched to specific mode pairs, and ℓ is a data sample index. For example, ℓ may refer to sound recordings from a specific ship on a specific array.

The waveguide invariant $\beta_{n,m}$ for modes n and m can be defined as[16,17]

$$\beta_{n,m}(\omega) = \frac{\eta_{nm}(\omega)}{\zeta_{nm}(\omega)}, \quad (12)$$

where

$$\eta_{n,m}(\omega) = \frac{1}{c_n(\omega)} - \frac{1}{c_m(\omega)}, \quad (13)$$

$$\zeta_{n,m}(\omega) = \frac{1}{v_n(\omega)} - \frac{1}{v_m(\omega)}. \quad (14)$$

The modal phase speed of the nth mode is defined as

$$c_n(\omega) = \frac{\omega}{k_n(\omega)}, \quad (15)$$

and the group velocity for mode n is defined as

$$v_n = \left[\frac{\partial}{\partial\omega}k_n(\omega)\right]^{-1}. \quad (16)$$

C. Feature-based maximum entropy

Jaynes' maximum entropy method[23–25] as applied to data ensembles provides a means to compute a conditional posterior probability distribution $P(\theta_\ell|\vec{\mathfrak{F}}_\ell, \mathfrak{M})$ for each data sample $\vec{\mathfrak{F}}_\ell$, where the notation $P(\theta_\ell|\vec{\mathfrak{F}}_\ell, \mathfrak{M})$ implies an estimate of $\mathfrak{M}$ is made prior to the use of data $\mathfrak{F}$. The notation θ_ℓ denotes a model parameter space that is connected to a data sample $\vec{\mathfrak{F}}_\ell$. The statistical inference method used in this analysis is defined by a *canonical* distribution,[26–28]

$$P(\theta_\ell|\vec{\mathfrak{F}}_\ell, \mathfrak{M}) = P(\theta_\ell, \mathfrak{M})\frac{\exp\left[-\mathrm{b}_\ell E_\ell(\theta_\ell, \vec{\mathfrak{F}}_\ell), \mathfrak{M}\right]}{Z_\ell}, \quad (17)$$

where Z_ℓ and b_ℓ are the partition function and the Boltzmann factor, respectively, with

$$Z(\beta_\ell, \mathfrak{M}) = \int d\theta P(\theta, \mathfrak{M})\exp\left[-\mathrm{b}_\ell E_\ell(\theta_\ell, \vec{\mathfrak{F}}_\ell), \mathfrak{M}\right]. \quad (18)$$

The error function E_ℓ used in this analysis includes a summation over the multiple singular points k found for data sample ℓ,

https://doi.org/10.1121/10.0010372

$$E_\ell(\theta_\ell, \vec{\mathfrak{F}}_\ell, \mathfrak{M}) = \sum_k (M_k(\theta, \mathfrak{M}) - {}^\ell\mathcal{F}_k)^2, \tag{19}$$

where $M_k(\theta, \mathfrak{M})$ is the modeled value of the frequencies where the group velocities of specified mode pairs become equal. Also, $\langle E_\ell \rangle$ is estimated as

$$\langle E_\ell \rangle \approx \frac{1}{K} \sum_j E(\hat{\theta}_\ell, \vec{\mathfrak{F}}_j, \mathfrak{M}), \tag{20}$$

where $\hat{\theta}_\ell \in \theta_\ell$ such that $E(\hat{\theta}_\ell, \mathfrak{M}) \leq E(\theta_\ell, \mathfrak{M})$ for all θ_ℓ. The Boltzmann factor b_ℓ is determined by solving the constraint integral equation,

$$\langle E_\ell \rangle = \int d\theta_\ell \frac{\exp\left[-\mathrm{b}_\ell E(\theta_\ell, \vec{\mathfrak{F}}_\ell)\right]}{Z_\ell(\mathrm{b}_\ell)} E_\ell(\theta_\ell, \vec{\mathfrak{F}}_\ell, \mathfrak{M}). \tag{21}$$

In the case where the posterior distribution has a Gaussian shape, $\mathrm{b}_\ell = 1/2\sigma_\ell$, where σ_ℓ is a standard deviation.

It is important to note that $\langle E_\ell \rangle$ is an average over elements of $E(\hat{\theta}_\ell, \vec{\mathfrak{F}}_j, \mathfrak{M})$ that contain the optimal error function value for the sample $\vec{\mathfrak{F}}_\ell$ and the off diagonal terms. If the off diagonal terms vanish, b_ℓ becomes infinite, and thus the marginal solutions would become delta functions, i.e., there would be no uncertainty. Specifically, it is the off diagonal terms that provide a finite uncertainty to marginal distributions.

IV. ANALYSIS

A. Singular point classification and assignment

At the center of the statistical inverse problem examined in this paper is the proposed use of certain types of features that can be extracted from broadband acoustic data commonly available around shipping lanes in shallow water for the purpose of inferring geoacoustic parameter values for a modeled seabed. The challenge is that a data processing stream that extracts the singular points of the waveguide invariant for specific pairs of mode numbers needs to be correctly identified. However, the identification of the mode pairs requires an *a priori* waveguide model, including a model for the seabed, which is the very goal of the feature-based inversion in the current paper. Mathematically, this is a non-linear problem, not unlike the Hartree–Focke problem in nuclear structure,[29] and the general approach to such problems is an iterative method with the hope of a convergent process. But the problem is even more complicated because generally this in itself is a non-deterministic problem. In a way, this is a statistical coupled problem between two domains, (1) pairs of modes and (2) geoacoustic parameter values, where both domains depend on a model space $\mathfrak{M}$.

At this stage, no simple automated method is available to associate an observed singular point in a spectrogram (such as those shown in Figs. 2 and 3) with a specific mode pair, which is similar in scope to the problem of identifying multipaths in sonar array signal processing. Generally, multipath identification is an iterative process and as such is a non-linear problem where convergence is not guaranteed. This section focuses on a subset of singular points, labeled as class I singularities, whose identification appears to be unique using a simple two-layer model and on the fact that a sparse number of these singularities in themselves contain useful information about the SBCEXP seabed, such as the sound speed in these two layers. This approach effectively decouples the two stochastic domains, allowing the random parameter space to be defined by the seabed parameters of $\mathfrak{M}$.

This section also discusses another set of singularities, called class II, where the mode pair identification is significantly more complicated because of a stronger dependence on the detailed nature of the deeper sediment layers. For these higher order singularities, the feature data identification problem becomes probabilistic as opposed to deterministic, which is why for this study class II and higher order singularities are excluded in selecting data samples of singular points for the ensemble maximum entropy analysis. Potentially, a convolutional neural network (CNN) such as that used by Van Komen *et al.*[30] could facilitate the process in a manner where all classes of waveguide invariant singularities are processed, but such an application is beyond the scope of the current study.

A preliminary geoacoustic profile is shown in Table I that, when used as an input into a normal mode model[31,32] along with a measured sound speed profile, allows for a prediction of $\beta_{m,n}(f)$ in Eq. (12) and the time-frequency spectrogram received level $\mathrm{RL}_{\mathrm{mod}}(f)$ in Eq. (6). These assumed geoacoustic parameter values for the mud layer were obtained from an analysis[33] of continuous wave (CW) transmission data measured on the MPL VLAs from a towed source emitting sound in the 1500–4000 Hz band. The analysis in Ref. 33 utilized the Buckingham viscous grain shearing (VGS) model for the seabed.[34] A 3 m transition layer from the mud to the sand is included in the geoacoustic model and was originally observed in the cores taken from

TABLE I. Preliminary geoacoustic profile used to identify mode pairs for singular points of $\beta_{m,n}$. Between the sand layer and a basement half-space, there are three deep layers (DL), DL1, DL2, and DL3, respectively. For all layers, the sound speed in the ith + 1 layer is greater than in the ith layer.

Content	Mud	Transition	Sand	DL1	DL2	DL3	Basement
Layer thickness (m)	9.2	3.0	7.5	173.2	185	500	—
Sound speed (top) (m/s),	1445	1446	1750	1760.3	1900	2100	2350
Sound speed (bottom) (m/s)	1446	1750	1750	1760.3	1900	2100	2350
Density (km/m^3)	1.62	1.8	1.83	2.0	2.2	2.2	2.6
Attenuation [dB/(m/kHz)]	0.04	0.15	0.15	0.15	0.15	0.15	0.22

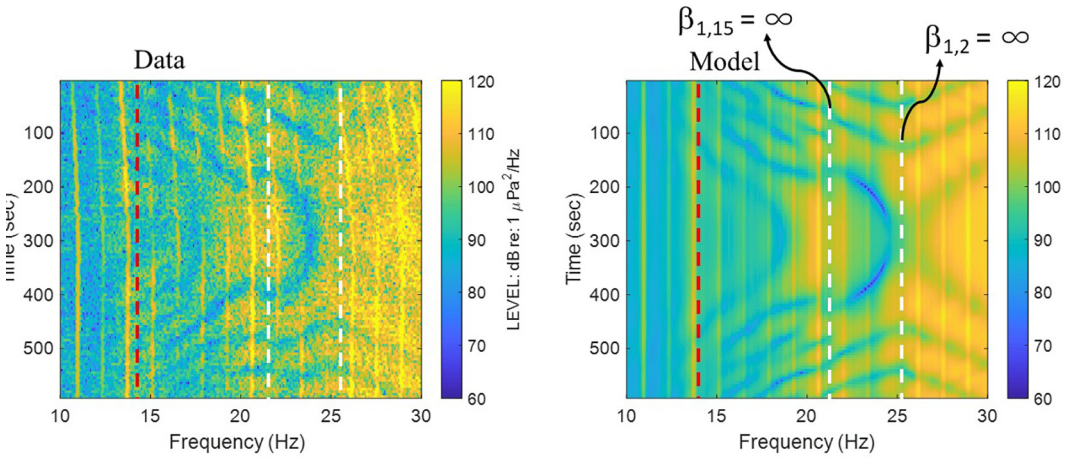

FIG. 4. (Color online) Model data comparison of time-frequency spectrogram during passage of the *KALAMATA* at a receiver depth 29.95 m on VLA 2. The geoacoustic profile is shown in Table I. The ship speed is 19.5 knots, and the CPA range is 3000 m. The assumed source depth is 9 m. The water depth was 75 m, and the sound speed profile was the measured profile closest in space and time to the acoustic measurements.

Twichell *et al.*[12] and also confirmed with the geophysical evidence discussed by Goff *et al.*[13] It is of interest to note that Belcourt *et al.*,[35] using a trans-dimensional inversion method, inferred a depth dependence that was consistent with observations by Twichell *et al.* and Goff *et al.*

The geoacoustic properties of the deep layers 1–3 (DL1–DL3) in Table I were ascertained in a *trial and error* mode of modeling the features of selected spectrograms for the *KALAMATA*. Figure 4 compares a modeled computation to the observed spectrogram shown in Fig. 2(a). The purpose of introducing DL2 and DL3 over the high speed basement was to predict the observed mode cutoff value of about 13.8 Hz for mode numbers $n > 1$. The thickness for DL2 was adjusted to give the observed singular points at 20.5 Hz seen in Fig. 4(a). The introduction of DL3 with the high basement sound speed had the effect of transforming a part of the horizontal wavenumber continuum into a discrete spectrum. In Fig. 4, the singular point of $\beta_{1,2}$ at about 25 Hz is evident.[8] For increasing frequencies, β approaches $+1$. However, in the 14–25 Hz band, one observes striations with $\beta \approx -1$. Also evident is the ability of the model to predict the striations down to about 14 Hz, where they vanish because of mode cutoff for mode number greater than one. To predict the $\beta_{1,2} = \infty$ feature observed at about 25 Hz on VLA 2 [Fig. 2(a)], the thickness of DL1 was set to 173 m with sound speed of about 1760 m/s.[8]

Using the preliminary geoacoustic profile in Table I, the singular points of Fig. 4 can be assigned to mode pairs. This step was accomplished by computing the modal group velocity and $\beta_{n,m}$ frequency dispersion curves and then matching the observed and modeled features in the spectrograms to specific singular points of $\beta_{n,m}$.

An example of the group velocities associated with the preliminary geoacoustic model is shown in Fig. 5 for low frequencies. The group velocities in Eq. (16) were computed using a five-point derivative of the horizontal wavenumber eigenvalues.[36] Two classes of singular point structures of $\beta_{n,m}$ for a mode pair m and n are observed. The first class of singular points (class I) are where the group velocity curves for modes $m = 2, 3, 4, \ldots$ intersect the mode 1 group velocity curve such that in the vicinity of the singular point,

$$\begin{aligned} v_m &> v_1 \quad \text{for } f < \mathcal{F}, \\ v_m &< v_1 \quad \text{for } f > \mathcal{F}, \end{aligned} \tag{22}$$

where $\mathcal{F}$ is the singular point frequency. The first four class I singular points ($\beta_{1,2}, \beta_{1,3}, \beta_{1,4}, \beta_{1,5}$) are shown as purple circles in Fig. 5. A second class of singular points

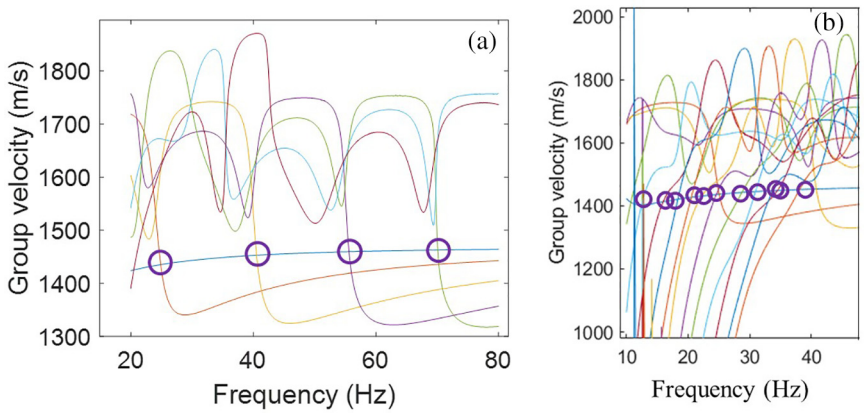

FIG. 5. (Color online) Modal group velocity curves versus frequency for the geoacoustic profile in Table I and a sound speed profile measured during SBCEXP 2017. Purple circles mark positions of singular points for (a) class I and (b) class II singularities.

https://doi.org/10.1121/10.0010372

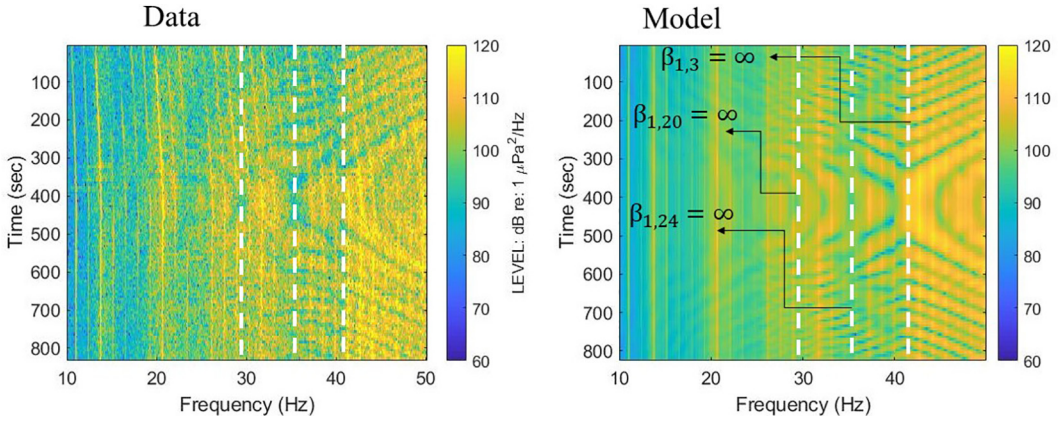

FIG. 6. (Color online) Model data comparison of time-frequency spectrogram during passage of the *KALAMATA* at a receiver depth 29.5 m on VLA 2. The geoacoustic profile is shown in Table I. The ship speed is 19.5 knots, and the CPA range is 3000 m. The assumed source depth is 9 m. The water depth was 75 m, and the sound speed profile was the measured profile closest in space and time to the acoustic measurements.

(class II) occur when the group velocity curves for modes $m = 2, 3, 4, \ldots$ intersect the mode 1 group velocity curve such that in the vicinity of the singular point,

$$\begin{aligned} v_m &< v_1 \quad \text{for } f < \mathcal{F}, \\ v_m &> v_1 \quad \text{for } f > \mathcal{F}. \end{aligned} \tag{23}$$

There are other classes. For example, class III is a generalization of class I,

$$\begin{aligned} v_m &> v_n \quad \text{for } f < \mathcal{F}, \\ v_m &< v_n \quad \text{for } f > \mathcal{F}, \end{aligned} \tag{24}$$

where $n < m$. For a single mode pair, $\beta_{n,m}$ may possess multiple singular points that belong to different classes, as is visible in Fig. 5. From Fig. 5, it is observed that singularities of $\beta_{1,m}$ $m = 2, 3, 4, 5\ldots$ belong to class I, whereas $\beta_{1,15}$ and $\beta_{1,24}$ belong to class II. Class I, II, and III singular points can all be observed in the merchant ship spectrograms measured during SBCEXP 2017. Figure 6 compares the measured and modeled spectrogram of sound recordings on VLA 2 during the passage of the *KALAMATA* that shows the class I singular point for $\beta_{1,3}$ and the class II singular points for $\beta_{1,20}$ and $\beta_{1,24}$. These class II singularities are observed on multiple ship data samples.

Using the geoacoustic profile in Table I and a measured SSP, plots of $\beta_{n,m}$ versus frequency were constructed, and they clearly show the difference in class I and class II singular points. Figure 7(a) shows predicted $\beta_{n,m}$ dispersion curves for mode pair correlations for class I and class II singular points for mode pairs (1,2), (1,3), (1,4), (1,5), (1,15), and (1,24). The modeled singular points for these pairs are approximately 25, 41, 55, 70, 21, and 35 Hz. These specific pairs of modes are of interest because of the apparent correspondence to the observed singular point values in Figs. 4 and 6. Figure 7(b) shows an enhanced view of $\beta_{1,15}$ and $\beta_{1,2}$, which illustrates that for class I (e.g., $\beta_{1,2}$), β goes to $-\infty$ prior to the singular point and to $+\infty$ just after the singular point. For class II singular points, β has the opposite behavior (e.g., $\beta_{1,15}$). For $\beta_{1,2}$, one observes that the singular structure is of the form of a derivative of the delta family (as $f \to 0+$),[37]

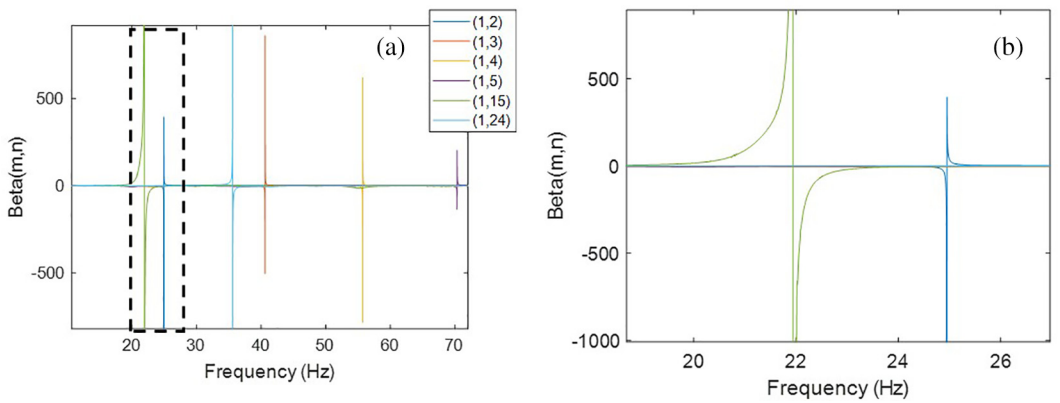

FIG. 7. (Color online) (a) $\beta_{n,m}$ versus frequency for the geoacoustic profile in Table I and a sound speed profile measured during SBCEXP 2017 for class I ($m = 1$, $n = 2,3,4,5$) and class II ($n = 1$, $m = 15$) and ($n = 1$, $m = 24$); (b) $\beta_{1,15}$ and $\beta_{1,24}$ on a larger scale that shows the difference in the singular point structure for class I versus class II singular points.

$$g_t(f) = \frac{e^{-f^2/4t}}{(4\pi t)^{1/2}}, \tag{25}$$

whereas the form for $\beta_{1,15}$ has the opposite sign,

$$g_t(f) = -\frac{e^{-f^2/4t}}{(4\pi t)^{1/2}}. \tag{26}$$

While there exists a unique association between class I modeled singularities and the observed singularities, the association of a class II singularity with an observed singularity is not unique. The difference occurs because as the depth and sound speed of the very deep layers increase, so too do the densities (number of modes per unit frequency) of modeled class II singular points. Thus, the association of a specific mode pair for a model class II singularity with an observed singular point depends on the *decision* of how deep to extend the sediment thickness and the sound speed in the basement half-space. In this study, only class I singularities, along with the mode-cutoff constraint, are utilized to infer the statistical properties of selected geoacoustic parameter values. In summary, the values of the very deep layers and basement sound speeds in Table I were adjusted to reproduce these VLF features and not the data used in the statistical inference problem, which are the class I singularities.

Figure 8 compares the measured and modeled spectrogram of sound recordings on VLA 2 during the passage of the *KALAMATA*. The observed singular point at about 53 Hz is assigned $\beta_{1,4}$ from the modeled spectrogram and a corresponding group velocity curve such as that shown in Fig. 7. The modeled spectrogram was made using a modified version of the geoacoustic profile in Table I. The modification is in DL1, where the sound speed and layer thickness are changed to 1810 m/s and 271 m, respectively. These parameter values were previously reported in Ref. 8 to predict the singular point for $\beta_{1,2}$ observed on VLA 1, which was 22.5 Hz instead of the value of 25 Hz observed on VLA 2. With this modification of DL1, the singular point value for $\beta_{1,4}$ is lowered from about 55.5 to 53 Hz, in good agreement with the observed singular point value and also resulting in a good fit to the measured RL. However, as noted, the modified geoacoustic model predicts a singular point value for $\beta_{1,2}$ of about 22.5 Hz, which differs from the observed singular point value of about 25 Hz on VLA 2. Namely, the model–data agreement shown in Fig. 4 cannot be achieved with the modified geoacoustic model. Many attempts were made to fit both the measured singular point values for $\beta_{1,4}$ and $\beta_{1,2}$, but to no avail. A tentative conclusion is that the seabed over which the propagation paths from points on the track of the *KALAMATA* to VLA 2 is not horizontally stratified. The presumed model error associated with not properly including non-horizontal layering is a source of uncertainty in this study. There are other explanations, but there exists geophysical information from the Siegel survey[38] data that supports this point.

A study of the merchant ship recordings made during SBCEXP 2017 on MPL VLA 2 other than that of the *KALAMATA* yielded four class I data samples. VLA 2 was well-positioned because CPA ranges were 2.5–4.5 km as compared to CPA ranges for VLA 1, which were 6–8 km. Further, measured class I singular points for mode pairs $(1,3)$ and $(1,4)$ derived from acoustic recordings of noise on VLA 2 from the *VIKING BRAVERY* are included in the total number of observed singular points. For the *VIKING BRAVERY*, the source level below 25 Hz was insufficient to make a definitive identification of $\beta_{1,2}$. The signal-to-noise ratios of acoustic data processed on VLA 1 for sound recordings of the *VIKING BRAVERY* were unfortunately insufficient to identify the singular points for mode pairs (1,3) and (1,4). The observed singular points from the spectrograms of the *TORM CORRIEDO*, the *MAERSK MATSUYAMA*, the *HAFNIA*

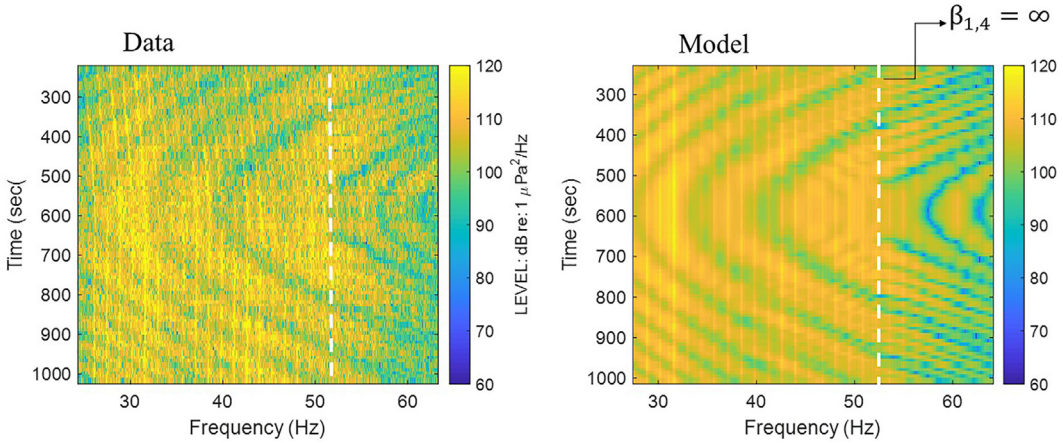

FIG. 8. (Color online) Model data comparison of time-frequency spectrogram during passage of the *KALAMATA* at a receiver depth 29.95 m on VLA 2. The geoacoustic profile is shown in Table I. The ship speed is 19.5 knots, and the CPA range is 3000 m. The assumed source depth is 9 m. The water depth was 75 m, and the sound speed profile was the measured profile closest in space and time to the acoustic measurements The measured spectrogram was derived from the same sound recording as in Fig. 4, but over a larger time interval and different frequency band.

https://doi.org/10.1121/10.0010372

TABLE II. Geoacoustic model $\mathfrak{M}$ used to compute a posterior probability distribution.

Content	Mud	Transition	DL1	DL2	DL3	Basement
Layer thickness (m)	9.2	3.0	T_{DL1}	185	500	—
Sound speed (top) (m/s)	C_M	C_M	C_{DL1}	1900	2100	2350
Density (km/m^3)	1.62	1.8	2.0	2.2	2.2	2.6
Attenuation [dB/(m/kHz)]	0.04	0.15	0.15	0.15	0.15	0.22

GREEN, and the *VIKING BRAVERY*, with their data samples $\vec{\mathfrak{F}}_{\ell=1}$, $\vec{\mathfrak{F}}_{\ell=2}$, $\vec{\mathfrak{F}}_{\ell=3}$, $\vec{\mathfrak{F}}_{\ell=4}$ (in Hz), respectively, are

$$\begin{aligned}
\vec{\mathfrak{F}}_{\ell=1} &= (25.0(1,2), 40.9(1,3), 53.7(1,4)),\\
\vec{\mathfrak{F}}_{\ell=2} &= (25.0(1,2), 40.7(1,3), 53.7(1,4), 69.86(1,5)),\\
\vec{\mathfrak{F}}_{\ell=3} &= (25.3(1,2), 41.8(1,3), 53.8(1,4)),\\
\vec{\mathfrak{F}}_{\ell=4} &= (40.5(1,3), 55.3(1,4)).
\end{aligned} \tag{27}$$

B. Results

With only a sparse number of class I singular features (12 points), the geoacoustic model in Table I was simplified by merging the 7.5 m sand layer into the DL1 layer. The hypothesis space of this simplified geoacoustic model consists of the sound speed and sediment thickness for DL1 and the sound speed in the mud layer.[39,40] Table II shows the simplified model and the upper and lower bounds of the geoacoustic parameters that are considered as random parameters. It is assumed that the prior probability distribution between the lower and upper bounds for the random parameters is a uniform distribution. The lower and upper bounds for the sound speed in DL1 were 1750 and 1850 m/s, respectively. The lower and upper bounds for the sediment thickness in DL1 were 100 and 300 m, respectively. The lower and upper bounds for the sound speed in the mud were 1435 and 1749 m/s, respectively. The reason that the lower and upper bounds for the *mud* layer spans fine to coarse grained sediment water-saturated sound speeds is that this study wanted to test the degree of information about the surface sediment layer contained in a sparse number of class I waveguide invariant singular points. All other parameters in Table II are held fixed.

For each data sample, the error function [Eq. (19)] was sampled with 15 000 Monte Carlo iterations for the three-parameter space between the specified upper and lower parameter value bounds. These samples were then used to compute the posterior probability distributions and multi-dimensional integrals in Eqs. (17), (18), and (21). Table III shows $E(\hat{\theta}_\ell\ (\ell = 1,2,3,4)\ , \vec{\mathfrak{F}}_j\ (j = 1,2,3,4))$. The average cost value $\langle E_\ell \rangle$ [Eq. (20)] for each data sample $\vec{\mathfrak{F}}_\ell$ is then utilized to compute $\mathfrak{b}_\ell$, which then makes the canonical distribution in Eqs. (17) and (18) unique.

TABLE III. The matrix $E(\hat{\theta}_\ell\ \ell = (1,2,3,4),\ \vec{\mathfrak{F}}_j j = (1,2,3,4))$. The diagonal elements are the optimized cost values $E(\hat{\theta}_\ell)$.

Data sample	*TORM CORRIEDO*	*MAERSK MATSUYAMA*	*HAFNIA GREEN*	*VIKING BRAVERY*	$\langle E \rangle$	$\mathfrak{b}$
TORM CORRIEDO	2.74	2.90	2.96	3.25	2.87	13.8
MAERSK MATSUYAMA	2.22	2.14	2.69	2.62	2.35	8.0
HAFNIA GREEN	4.33	4.23	4.09	4.20	4.21	13.6
VIKING BRAVERY	0.500	0.190	0.068	0.012	0.040	42

The use of Eq. (20) assumes that each data sample is from the same statistical ensemble. A cursory examination of the elements of E in Table III suggests that there are two groups: $\vec{\mathfrak{F}}_{\ell=1,2,3}$ with three elements and $\vec{\mathfrak{F}}_{\ell=3,4}$ with two elements. The main basis for this grouping is the observation discussed with respect to Fig. 4 that leads one to a supposition of an unknown horizontal dependence in two dimensions of the properties of DL1 that has a strong effect on the singular point spectrum of $\beta_{1,n}$, $n = 2,3,4$. The data sample $\ell = 3$ for the *HAFNIA GREEN* appears to belong in both the first and second group. Other than the CPA of the *HAFNIA GREEN* relative to VLA 2 being closest to the CPA of the *VIKING BRAVERY*, as compared to the *MAERSK MATSUYAMA* and the *TORM CORRIEDO*, there is insufficient prior information about the layering of the mud and sand layers to go beyond this proposed grouping. In summary, $\langle E_{\ell=1,2,3} \rangle$ is formed via a sum in Eq. (20) over $j = 1, 2, 3$, and $\langle E_{\ell=3,4} \rangle$ is formed via a sum in Eq. (20) over $j = 3, 4$. It is not surprising that $\mathfrak{b}_{\ell=4}$ is large because there are only two elements in $\vec{\mathfrak{F}}_{\ell=4}$.

Figure 9 shows marginal probability distributions for C_{mud}, C_{DL1}, and T_{DL1} inferred from the *MAERSK MATSUYAMA* data sample. The peak values of the pair

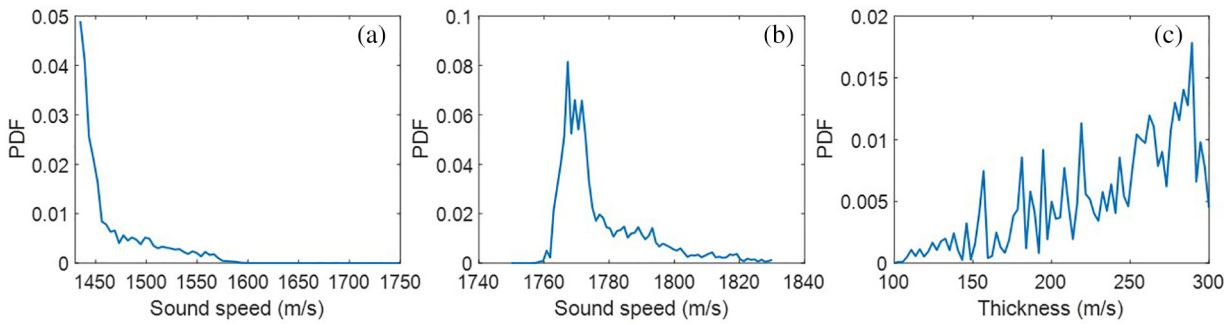

FIG. 9. (Color online) Marginal probability distributions inferred from the *MAERSK MATSUYAMA* data sample for (a) C_{mud}, (b) C_{DL1}, and (c) T_{DL1}.

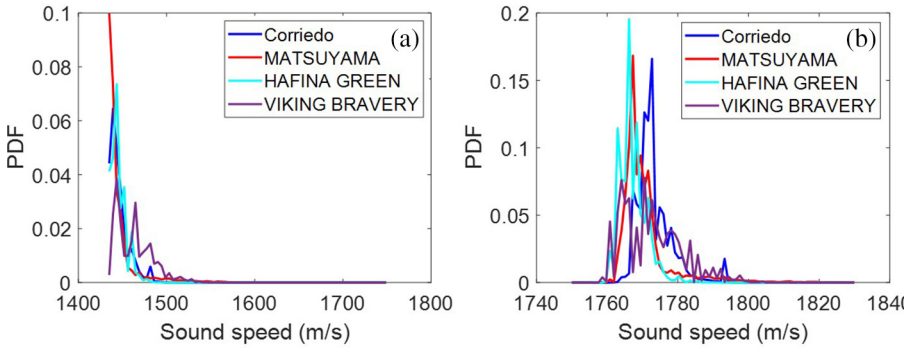

FIG. 10. (Color online) Marginal probability distributions inferred for (a) C_{mud} and (b) C_{DL1} for data samples for the *TORM CORRIEDO*, the *MAERSK MATSUYAMA*, the *HAFNIA GREEN*, and the *VIKING BRAVERY*.

distribution function (PDF) for C_{mud}, C_{DL1}, and T_{DL1} are 1435 m/s, 1767 m/s, and 290 m, respectively. The distribution for C_{mud} is sharply peaked at the lower bound and thus highly asymmetrical, which leads to an average value of about 1445 m/s that is greater than the peak value of the PDF. On the other hand, the PDF for C_{DL1} is sharply peaked with its peak value (1767 m/s) near the average (1771 m/s). The distribution for T_{DL1} is peaked near the upper bound and thus highly asymmetrical. It was found that for all the data samples, T_{DL1} had this general shape shown in Fig. 9.

As a comparison of the results from different data samples, Fig. 10 shows marginal probability distributions for C_{mud} and C_{DL1} inferred from the *TORM CORRIEDO*, the *MAERSK MATSUYAMA*, the *HAFNIA GREEN*, and the *VIKING BRAVERY* data samples. Table IV summarizes the statistical measures for C_{mud} and C_{DL1}. The averages of the peak value of the PDF for C_{mud} and C_{DL1} are 1439 and 1773 m/s, respectively. For the mud sediment, this gives an average sound speed ratio (SSP) = 1439/1471 = 0.978, which compares to 0.975 in Ref. 28. The average of the sound speed in the deep layer beneath the mud layer at the peak of the marginal probability distribution is about 1770 m/s, which is consistent with Siegel *et al.*,[39] who suggest a deep low speed layer that extends to a depth of about 300 m beneath the seabed.

The mean values of C_M, C_{DL1}, and T_{DL1} inferred from the low-frequency singularities can reproduce the measured features across a wider band. Figure 11 shows modeled and measured RLs in the 15–200 Hz band for sound recordings of the passage of the *VIKING BRAVERY* on VLA 2. Thus, this computation examines part of the frequency spectrum, 70–200 Hz, not used in the analysis. The normal mode model uses the optimal geoacoustic model $\hat{\theta}_{\ell=4}$ belonging to the feature vector $\tilde{\mathfrak{F}}_{\ell=4}$. The CPA range and the ship speed are about 3.19 km and 17.0 knots, respectively. The source levels $\text{SL}(f)$ are computed using Eq. (15). Overall, the modeled and measured spectrograms are in qualitative agreement.

V. SUMMARY AND DISCUSSION

The observed singular points of the mode-pair waveguide invariant $\beta_{n,m}(f)$, $n, m = 1, 2, \ldots, N$, where N is the number of modes, were used to develop a low-frequency (15–80 Hz) feature-based statistical inference method. The specification of prior geoacoustic information included the insertion of very deep layers with sound speeds and attenuations that when used in a normal mode propagation model simulated the observed striations at frequencies below 20 Hz. The model space consisted of sound speed in a layer of mud, a sound speed for a water-saturated sand layer beneath a transition layer that separates the mud from the sand, and a sediment thickness for the sand layer. The sediment thickness of the mud layer (9.2 m) and of the transition layer (3 m) were assumed known from previous studies.

Using a feature-based cost function for data samples, marginal probability distributions were computed using a maximum entropy approach. Four data samples were used in the inversion. The low-frequency sound recordings from multiple merchant ships provided data samples with singular points for $\beta_{1,2}$, $\beta_{1,3}$, $\beta_{1,4}$, and $\beta_{1,5}$ on VLA 2. While the singular points are sparse, they form a pattern that provides a sufficient amount of evidence to extract statistics of the sound speed within the mud and the sediment layer beneath. The deeper portions of the sediment were specified directly by introducing very deep layers and a sufficiently high sound speed that allows the modeled spectrograms to possess striations down to about 14 Hz.

The resulting marginal probability distributions for the mud layer above a transition layer clearly demonstrate a high likelihood of a SSP that is less than unity. The average peak of the PDF for the sound speed of mud above the transition layer is located at about 1440 m/s. The average peak of the PDF for the sound speed beneath the mud + transition layer is located at about 1770 m/s.

TABLE IV. Sound speeds at the peak value of PDF and average and standard deviations for the mud layer and DL1.

Statistical measure	*TORM CORRIEDO*	*MAERSK MATSUYAMA*	*HAFNIA GREEN*	*VIKING BRAVERY*	Average
max $P_{C\text{mud}}$ (m/s)	1438	1435	1441	1441	1438.8
$\langle C_{\text{mud}} \rangle \pm \sigma$ (m/s)	1447 ± 11	1446 ± 20	1445 ± 9	1463 ± 21	1450 ± 13
max $P_{C\text{DL1}}$ (m/s)	1773	1767	1766	1771	1769.3
$\langle C_{\text{DL1}} \rangle \pm \sigma$ (m/s)	1773 ± 5	1771 ± 8	1767 ± 4	1772 ± 8	1770 ± 6

https://doi.org/10.1121/10.0010372

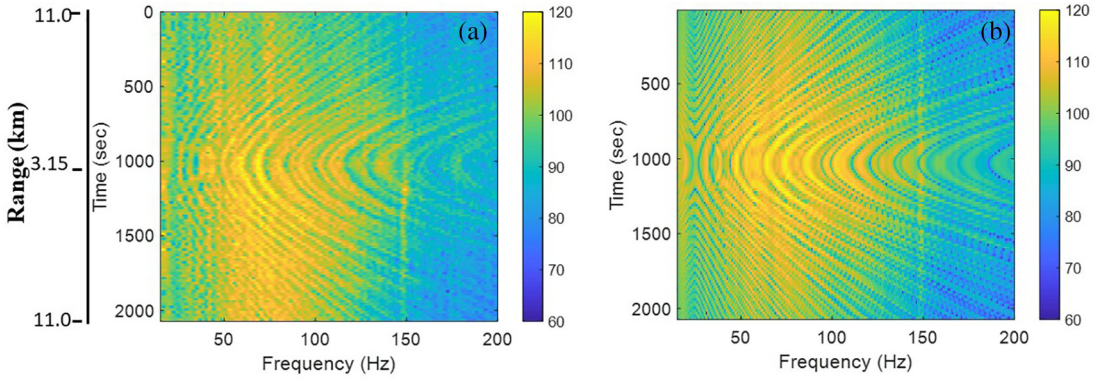

FIG. 11. (Color online) Comparison of (a) measured and (b) modeled spectrograms from the passage of the *VIKING BRAVERY* on VLA 2. Comparison was made in the 15–200 Hz bands. The CPA range is about 3190 m, and the ship speed is about 17 knots. The source and receiver depth are 9.3 and 41.2 m, respectively. The geoacoustic model is that of Table III with C_M, C_{DL1}, and T_{DL1} taken as the peak values of the PDF for the *VIKING BRAVERY* data sample of two singular points.

The low-frequency approach has two main limitations. First, because of the sparseness of the data set, the size of the parameter space must remain small to avoid overfitting. Second, the current approach requires a preliminary geoacoustic model along with a normal mode propagation model with which to identify the modal pairs that belong to a specific observed singularity. Currently, the normal mode approach assumes that the ocean waveguide and seabed are horizontally stratified.

The frequencies at which singular points in β occur that characterize the acoustics of a seabed are analogous to the chords of a musical melody. For example, for the *MAERSK MATSUYAMA*, there are four singular points identified for the New England Mud Patch. These singular points are analogous to the four chords A, A7, D, A that characterize in part the song *Get Back* by the Beatles.[41]

[1]G. V. Frisk and J. F. Lynch, "Shallow water waveguide characterization using the Hankel transform," J. Acoust. Soc. Am. **76**, 205–216 (1984).
[2]S. Rajan, J. F. Lynch, and G. V. Frisk, "Perturbative inversion methods for obtaining bottom geoacoustic parameters in shallow water," J. Acoust. Soc. Am. **82**, 998–1017 (1987).
[3]K. M. Becker and G. V. Frisk, "The impact of water column variability on horizontal wave number estimation and mode based geoacoustic inversion results," J. Acoust. Soc. Am. **123**, 658–666 (2008).
[4]W. A. Kuperman and F. Ingenito, "Spatial correlation of surface generated noise in a stratified ocean," J. Acoust. Soc. Am. **67**, 1988–1996 (1980).
[5]C. H. Harrison and D. G. Simons, "Geoacoustic inversion of ambient noise: A simple method," J. Acoust. Soc. Am. **112**, 1377–1389 (2002).
[6]D. R. Barclay, D. A. Bevans, and M. J. Buckingham, "Estimation of the geoacoustic properties of the New England Mud Patch from the vertical coherence of the ambient noise in the water column," IEEE J. Ocean. Eng. **45**, 51–59 (2020).
[7]D. R. Barclay and M. J. Buckingham, "Depth dependence of wind-driven, broadband ambient noise in the Philippine Sea," J. Acoust. Soc. Am. **133**, 62–71 (2013).
[8]D. P. Knobles, P. S. Wilson, W. A. Hodgkiss, and T. B. Neilsen, "Influence of seabed on very low frequency sound recorded during passage of merchant ships on the New England shelf," J. Acoust. Soc. Am. **149**(5), 3294–3300 (2021).
[9]P. S. Wilson, D. P. Knobles, and T. B. Neilsen, "An overview of the Seabed Characterization Experiment," IEEE J. Ocean. Eng. **45**, 1–13 (2020).
[10]H.-C. Chiang, R. L. Moses, and L. C. Potter, "Model-based Bayesian feature matching with application to synthetic aperture radar target recognition," Pattern Recognit. **34**, 1539–1553 (2001).
[11]E. T. Whittaker and G. N. Watson, *A Course of Modern Analysis*, 4th ed. (Cambridge University, Cambridge, UK, 1927), Chap. X.
[12]D. C. Twichell, C. E. McClennen, and B. Butman, "Morphology and process associated with the accumulation of the fine-grained sediment deposit on the Southern New England Shelf," J. Sediment. Petrol. **51**, 269–280 (1981).
[13]J. A. Goff, A. Reed, G. Gawarkiewicz, P. S. Wilson, and D. P. Knobles, "Stratigraphic analysis of a sediment pond within the New England Mud Patch: New constraints from high-resolution chirp acoustic reflection data," Mar. Geol. **412**, 81–94 (2019).
[14]J. Chaytor, M. Ballard, B. Buczkowski, J. Goff, K. Lee, A. Reed, and A. Boggess, "Measurements of geologic characteristics and geophysical properties of sediments from the New England Mud Patch," IEEE J. Ocean. Eng. (published online 2021).
[15]L. Bluestein, "A linear filtering approach to the computation of discrete Fourier transform," IEEE Trans. Audio Electroacoust. **18**, 451–455 (1970).
[16]D. Rouseff and R. C. Spindel, "Modeling the waveguide invariant as a distribution," AIP Conf. Proc. **621**, 137–148 (2002).
[17]Y. Le Gall and J. Bonnel, "Passive estimation of the waveguide invariant per pair of modes," J. Acoust. Soc. Am. **134**(2), EL230–EL236 (2013).
[18]D. Rouseff and L. M. Zurk, "Striation-based beamforming for estimating the waveguide invariant with passive sonar," J. Acoust. Soc. Am. **130**, EL76–EL81 (2011).
[19]S. S. Chuprov, "Interference structure of the sound field in a stratified ocean," in *Ocean Acoustics: Current Status*, edited by L. M. Brekhovskikh (Nauka, Moscow, 1982), pp. 71–91 (in Russian).
[20]V. M. Kuzkin, "Frequency shifts of the sound field interference pattern in a shallow sea," Acoust. Phys. **45**, 224–229 (2002).
[21]E. C. Shang, J. R. Wu, and Z. D. Zhao, "Relating waveguide invariant and bottom reflection phase-shift parameter *P* in a Pekeris waveguide," J. Acoust. Soc. Am. **131**, 3691–3697 (2012).
[22]C. H. Harrison, "The relation between the waveguide invariant, multipath impulse response, and ray cycles," J. Acoust. Soc. Am. **129**, 2863–2877 (2011).
[23]E. T. Jaynes, *Probability Theory: The Logic of Science* (Cambridge University, Cambridge, UK, 2003), Chap. 10.
[24]E. T. Jaynes, "Information theory and statistical mechanics," Phys. Rev. **106**, 620–630 (1957).
[25]E. T. Jaynes, "Information theory and statistical mechanics: II," Phys. Rev. **108**, 171–190 (1957).
[26]L. E. Reichl, *A Modern Course in Statistical Physics*, 4th ed. (Wiley VCH, Berlin, 2016).
[27]D. P. Knobles, J. D. Sagers, and R. A. Koch, "Maximum entropy approach for statistical inference in an ocean acoustic waveguide," J. Acoust. Soc. Am. **131**, 1087–1101 (2012).

[28]D. P. Knobles, "Maximum entropy inference of seabed attenuation parameters using ship radiated broadband noise," J. Acoust. Soc. Am. **138**, 3563–3575 (2015).
[29]P. Ring and P. Schuck, *The Nuclear Many-Body Problem* (Springer-Verlag, New York, 1980), Chap. 5.
[30]D. F. Van Komen, T. B. Neilsen, D. B. Mortenson, M. C. Acree, D. P. Knobles, M. Badiey, and W. S. Hodgkiss, "Seabed type and source parameters predictions using ship spectrograms in convolutional neural networks," J. Acoust. Soc. Am. **149**, 1198–1210 (2021).
[31]E. K. Westwood, C. T. Tindle, and N. R. Chapman, "A normal mode model for acoustoelastic ocean environments," J. Acoust. Soc. Am. **100**, 3631–3645 (1996).
[32]E. K. Westwood and R. A. Koch, "Elimination of branch cuts from the normal mode solution using gradient half spaces," J. Acoust. Soc. Am. **106**, 2513–2523 (1999).
[33]D. P. Knobles, C. D. Escobar-Amado, M. J. Buckingham, W. S. Hodgkiss, P. S. Wilson, T. B. Neilsen, J. Yang, and M. Badiey, "Statistical inference of sound speed and attenuation dispersion of a fine-grained marine sediment," IEEE J. Ocean. Eng. (published online 2021).
[34]M. J. Buckingham, "Wave speed and attenuation profiles in a stratified marine sediment: Geo-acoustic modeling of seabed layering using the viscous grain shearing theory," J. Acoust. Soc. Am. **148**, 962–974 (2020).
[35]J. Belcourt, C. W. Holland, S. E. Dosso, J. Dettmer, and J. A. Goff, "Depth-dependent geoacoustic inferences with dispersion in the New England Mud Patch via reflection coefficient inversion," IEEE J. Ocean. Eng. **45**, 69–91 (2020).
[36]M. Abramowitz and I. A. Stegun, *Handbook of Mathematical Functions: With Formulas, Graphs, and Mathematical Tables* (Cambridge University, Cambridge, UK, 1972).
[37]I. Stakgold, *Green's Functions and Boundary Value Problems* (Wiley, New York, 1979), Chap. 2.
[38]J. Siegel, D. Lizarralde, B. Dugan, and M. Person, "Glacially generated overpressure on the New England continental shelf: Integration of full-waveform inversion and overpressure modeling," J. Geophys. Res. **119**, 3393–3409, https://doi.org/10.1002/2013JB010278 (2014).
[39]J. Yang and D. Jackson, "Measurement of sound speed in fine-grained sediments during the Seabed Characterization Experiment," IEEE J. Ocean. Eng. **45**, 39–50 (2020).
[40]D. P. Knobles, P. S. Wilson, J. Goff, L. Wan, M. J. Buckingham, J. D. Chaytor, and M. Badiey, "Maximum entropy derived statistics of sound speed structure in a fine-grained sediment inferred from sparse broadband acoustic measurements on the New England continental shelf," IEEE J. Ocean. Eng. **45**(1), 161–173 (2020).
[41]The Beatles, *The Beatles Anthology* (Chronicle Books, San Francisco, CA, 2000).